Laser assisted joining of St12 to polycarbonate: Experimental study and numerical simulation

Shaikh Mohammad Meiabadi, M. S., Kazerooni, A., Moradi, M. & Torkamany, M. J.

Original citation & hyperlink:
Shaikh Mohammad Meiabadi, MS, Kazerooni, A, Moradi, M & Torkamany, MJ 2020, 'Laser assisted joining of St12 to polycarbonate: Experimental study and numerical simulation', Optik, vol. 208, 164151.
https://dx.doi.org/10.1016/j.ijleo.2019.164151

DOI 10.1016/j.ijleo.2019.164151
ISSN 0030-4026

Publisher: Elsevier

Laser Assisted Joining of St12 to Polycarbonate; Experimental Study and Numerical Simulation

M.Saleh Shaikh Mohammad Meiabadi[1], Afshin Kazerooni[1], Mahmoud Moradi[2,3], M Javad Torkamany [4]*
1- Department of Mechanical Engineering, Faculty of Engineering, SRTT University, Tehran, Iran
2- Department of Mechanical Engineering, Faculty of Engineering, Malayer University, Malayer, Iran
3- Laser Materials Processing Research Center, Malayer University, Malayer, Iran
4- Iranian National Center for Laser and Technology, Tehran, Iran Po Box 14665-576
**Corresponding author: E-mail: moradi.malayeru@gmail.com*

Abstract
In this study dissimilar joining of St12 to Polycarbonate is accomplished by a Nd: YAG pulsed laser and examined by finite element (FE) model and analysed by statistical method. Several experiments are carried out to materialize a direct joint between St12 to Polycarbonate. To investigate thermal phenomena of the laser joining process a FE model is developed by Abaqus software. To approximate heat source distribution, a Cylindrical-Involution-Normal model is programmed in FORTRAN language. To find out the sensitivity of the FE model to the elements size, a number adjustment tests are used and the FE model is validated by experimental data. Effects of laser power (190-230 W) and laser scanning speed (3.6-7.6 mm/s) on average bond width (AW), delta bond width (DW), and maximum of temperature profile (MT) have been investigated via response surface methodology. Results reveal that power of laser is the determinant variable of average bond width and maximum temperature profile, however, scanning speed of laser is the most effective variable on delta bond width. An appropriate process window required to achieve a sound dissimilar joint (without any decomposition of the polymer) is finally suggested.

Keywords: Laser Assisted Metal and Plastic joining; St12; Polycarbonate; Numerical analysis; Finite Element Method

1-Introduction
Light metals and thermoplastics are being used in various industries namely automotive, aerospace, and medical equipment because of compatible mechanical and physical properties. There is a vital need to join dissimilar materials in hybrid structures. Many joining processes have been recently developed for joining metals to polymers and composite materials, including Friction Assisted Welding, Friction Spot Welding, Ultrasonic Joining, etc. Assembly techniques include mechanical joining processes and adhesive bonding. There are also different mechanical joining processes like screwing, snap joints, clinching, riveting just to name a few. However, stress concentration and unbalanced load distribution caused by hole drilling are unfavourable characteristics of the mechanical joining processes. In addition, the plastic and metal must be thicker generally to accommodate the stress concentrations at the hole and fastener point loads. Therefore, mechanical joints are not fully in compliance with the idea of lightweight joints. Automotive industries are now pledged to reduce fuel consumption based on government rules in many countries. A suitable way to reduce fuel consumption is, thus to

decrease weight of cars structures and their joints. Adhesive bonding is more suitable for large area joining parts [1] and also many adhesives require curing time to develop enough strength. All these joining processes require preparation steps and cannot be used in small integrated systems namely microelectromechanical systems. Laser materials processing is being utilised for various engineering applications namely cutting [2], hardnening [3], welding [4, 5] and brazing [6]. Laser joining has drawn substantial attention due to high quality, performance, speed, precision, suitable flexibility and low deformation or distortion [7]. Laser connecting of heterologous materials is a reliable solution for joining limitations of various joining processes [8]. The LAMP stands for the Laser Assisted Metal and Plastic joining process and was developed at the Osaka University. The LAMP process is a rapid, flexible and proficient solution to bond the entire surfaces of metals and plastics without any adhesive or mechanical joint. There are two procedures for laser beam joining of metals and polymers: Heat-conduction joining (HCJ) and Transmission joining (TJ). In TJ the plastic partner is transparent and thus can transmit the laser beam to heat the metal joining partner. As a result, the metal-plastic interface heats up to the point that the plastic is molten. Because of partial pyrolysis of the polymer small bubbles are formed. Activated high-temperature molten plastic which is in touch with the heated metal surface incurs high pressure thanks to the nucleation and development of the bubbles. Due to this pressure, the molten plastic is driven into metal surface cavities and it leads to a mechanical bonding. In addition, the polymer molecular chains form a chemical bond with surface metal oxide. Therefore, physical and chemical bonding between the metals and plastics is achieved. This procedure can only be applied to thermoplastics that have the ability to transmit electromagnetic radiation of the laser beam. HCJ is the well-suited joining procedure for plaque plastics. This method works independently of transparency of plastics since the metal surface is irradiated directly by the laser beam. The absorbed heat by metal surface is conducted to the plastic partner at the interface which leads to the melting of the plastic and pressurizing the molten polymr to the metal surface by developed bubbles and creating the dissimilar joint. Figure 1 represents the LAMP joining mechanisms. In the LAMP process, a strong joint can be produced by atomic, molecular bonding or nanostructural of the plastic and the metal through the oxide film on the surface of metal plate, where not only the anchor effect but also Van der Waals interaction forces and chemical bonding were expected [8, 9, 10]. Hence, laser connecting or joining is able to relieve the difficulties of typical polymer-metal connecting technologies [11]. The direct laser joining of engineering plastics and metals is taken into consideration to be developed in industrial applications [12, 13, 14, 15]. St12 (AISI 1008 Carbon Steel) is a low-carbon steel which has excellent weldability and formability. St12 is frequently used in automotive applications, home appliances, and furniture. Polycarbonate is widely used for automotive applications, medical devices, electronic components, aircraft, and packing. A comprehensive numerical and statistical investigation of the laser assisted joining of St12 to Polycarbonate is essential in order to obtain a suitable process window to reach a defect free dissimilar joint. In this research, St12 is directly joined to Polycarbonate for the first time by an Nd: YAG laser. A FE model is expanded to simulate laser connecting of St12 to Polycarbonate by ABAQUS software. Cylindrical-Involution-Normal (CIN) is also used to describe heat source power distribution in laser assisted metal to polymer connecting. The heat source model is programmed by the FORTRAN language. Moreover, the Finite Element model is validated by empirical results of the laser joining process. The Finite Element model is precisely capable of predicting temperature distribution of the joining process in the materials which primarily determines joint characteristics. In addition, effects of power and scanning speed of laser on the bond width variation and maximum of temperature profile are evaluated by FE model. The Response Surface Methodology (RSM) is exploited to carry out statistical

analysis and clearly determines effects of power and scanning speed of laser and their interactions on the average bond width, delta bond width, and maximum of temperature profile.

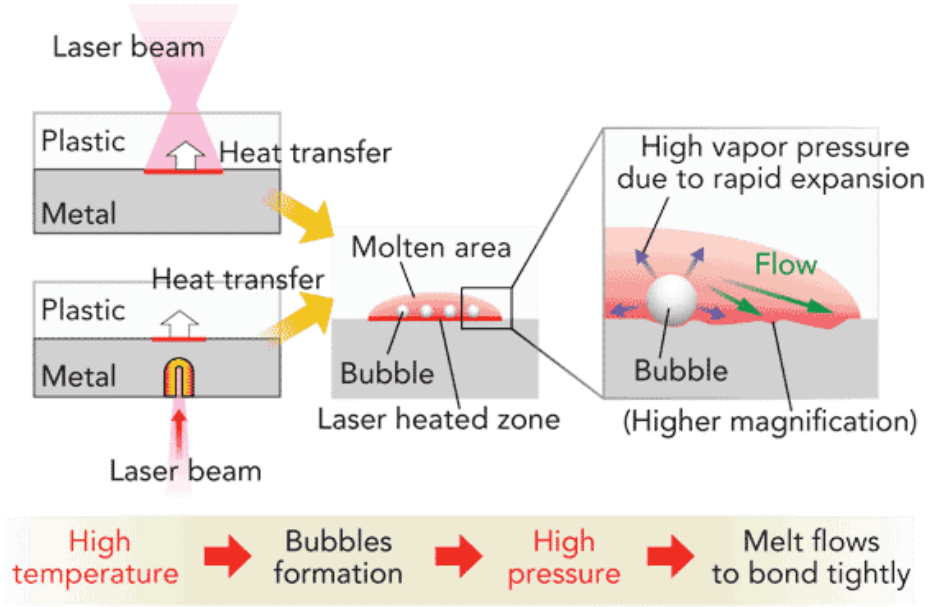

Fig. 1 Schematic representations of the LAMP joining mechanisms [7].

2- Methodology

2-1- Mathematical and Numerical Description

Heat source power distribution

An appropriate description of heat source power distribution is of great importance in numerical modelling of laser joining process since the shape of molten pool and the temperature distribution in the material are affected by heat source distribution [16]. The absorption of energy during laser joining process and the prompt transportation of the energy from surface into the workpiece is defined by two mechanisms of Fresnel's absorption and inverse Bremsstrahlung's absorption [17]. In numerical modelling of laser beam joining process Gussian distribution of the heat source is usually assumed in radial direction [18]. However, it was observed that absorption of energy decreases with the penetration of leasr beam into the material. Universal CIN heat source model gives a good approximation of distribution of volumetric heat source power. This model allows the description of volumetric heat source by considering heat source power density and material penetration depth. The CIN heat source is defined by the following equation [19]:

$$Q(r,z) = \frac{kK_z\eta_L\, Q_L}{\pi\left(1-e^{(K_z s)}\right)} e^{-\left(kr^2+K_z z\right)}\left(1-u(z-s)\right) \qquad (1)$$

Where Q_L is the power of laser beam, η_L is a laser efficiency, K_Z=3/s is an exponent of heat source power, r_0 is a radius of beam, k=3/r_0^2 is a coefficient of beam focus and s is the heat source beam penetration depth, u $(z\text{-}s)$ is Heaviside function. The FORTRAN software is applied to programme (CIN) heat source model. Moreover, in order to acquire a better understanding of thermal phenomena in laser joining process linear energy, L_e can be defined as ratio of laser beam power to laser speed. The following equation determines the linear energy:

$$L_e = \frac{Q_L}{v} \qquad (2)$$

Governing equations

The heat transfer modes which are included in this study are conduction in PC, St12, and fixture plates, convection and radiation surrounding in all parts, and gap conduction and radiation between PC and St12. For uniform and continuous media, the spatial and temporal temperature distribution T(x, y, z, t) satisfies the following differential equation for 3D heat conduction in a domain D [20]:

$$\frac{\partial}{\partial \mathrm{x}}\left(\mathrm{k_x(T)}\frac{\partial \mathrm{T}}{\partial \mathrm{x}}\right)+\frac{\partial}{\partial \mathrm{y}}\left(\mathrm{k_y(T)}\frac{\partial \mathrm{T}}{\partial \mathrm{y}}\right)+\frac{\partial}{\partial \mathrm{z}}\left(\mathrm{k_z(T)}\frac{\partial \mathrm{T}}{\partial \mathrm{z}}\right)+\mathrm{Q}=\rho \mathrm{c}\left(\frac{\partial \mathrm{T}}{\partial \mathrm{t}}-v\,\frac{\partial T}{\partial y}\right) \quad (3)$$

where *x, y, z* are the of the Cartesian coordinate values, *T* is the temperature (K), *kx, ky, kz* are the thermal conductivities in the *x, y* and *z* directions (W/(m K)), respectively, *Q* is the heat generation rate in per unit volume (W/(mK)), ρ is the material density (kg/m3), *c* is the specific heat capacity (J/(kgK)), *t* is the time (s), and *v* is the velocity of laser (m/s). The initial condition is written as follows:

$$T(x,y,z,0)=T_0 \quad for\ (x,y,z)\in D \quad (4)$$

The natural boundary condition are defined by:

$$k_n\frac{\partial T}{\partial n}-q+h(T-T_0)+\sigma\varepsilon(T^4-T_0^4)=0 \qquad (x,y,z)\in S \quad (5)$$

On the boundary *S* for *(x, y, z)* $\in$ *S* and *t*>0. *S* denotes those surfaces exposed to radiation, subjected to convection, and imposed heat fluxes. In addition, k_n represents the thermal conductivity (W/m K), *q* indicates the experimentally determined heat flux normal to *S* (W/m^2), h_{conv} is the convection heat transfer coefficient (W/m^2 K), σ is the Stefan–Boltzmann constant for radiation (5.67×10^{-8} W/m^2 K^4), ε is the emissivity, T_0 denotes the nodal temperature (K), and T_0 is the ambient temperature (K).

2-2- Finite Element Model Development

A FE model has been expanded by Abaqus software to simulate laser assisted St12 to Polycarbonate joining process. The FE model is a practical tool for mechanical and thermal analysis of the laser connecting process. In this FE model, St12 and Polycarbonate parts are meshed using coupled temperature-displacement elements to conduct thermal and mechanical analysis. The mesh pattern is also non-uniform to generate fine meshes along with laser travelling direction to predict accurate temperature distribution. Moreover, the coarse meshes are used in other parts of the 3D model as shown in Fig. 2 to avoid high simulation time.

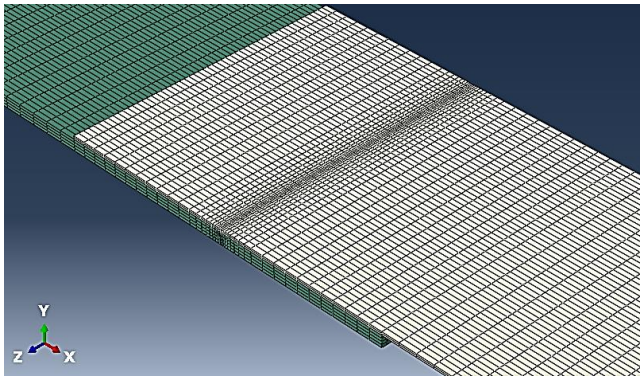

Fig. 2 Finite element mesh of St12 and Polycarbonate (width of samples = 40 mm)

To find out the sensitivity of the FE model to the size of elements, a number of element size adjustment tests are used. The material features of St12 and Polycarbonate used in the simulation are temperature dependent and are taked from literature [21, 22]. Natural and radiation convection have been evaluated for the boundary condition of heat transfer at all

directions open to neighboring. The joining time has been measured based on the scanning speed of laser and heat source location.

2-3- Numerical Analysis

The FORTRAN is linked to Abaqus to programme power distribution of heat source in the joining process. Laser joining is simulated with the process parameters as described below: laser beam power Q_L = 210 W, speed of laser v = 5.6 mm/s, spot size = 200 μm, laser efficiency η_L = 85% and the laser beam focused on the St12 surface. A 100 bar mechanical load with uniform distribution is applied by fixture plates on metal surface. Figure 3 demonstrates the temperature profiles after the temperatures have been stabilized on the Polycarbonate side transverse to the laser scanning direction. Acoording to the literature [22] the crystalline melting temperature range of Polycarbonate is (215-230°C) and decomposition temperature range of Polycarbonate is (377-462°C). The maximum temperature of this profile at the centre of the laser spot is lower than decomposition point of the Polycarbonate and therefore the bond width can be predicted by the zone that has gained temperatures higher than crystalline melting point of the Polycarbonate. The predicted bond width by temperature profile at the middle of laser travelling direction is 3.05 mm.

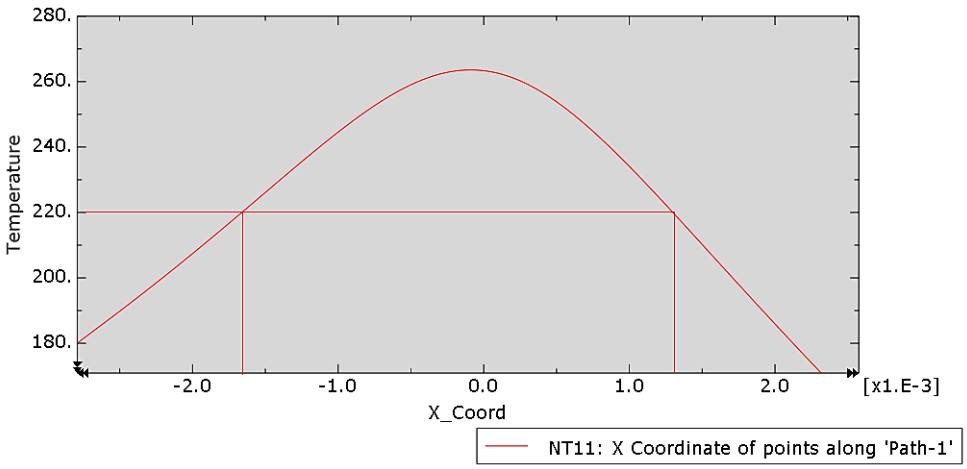

Fig. 3 Temperature profile transverse to the laser scanning direction

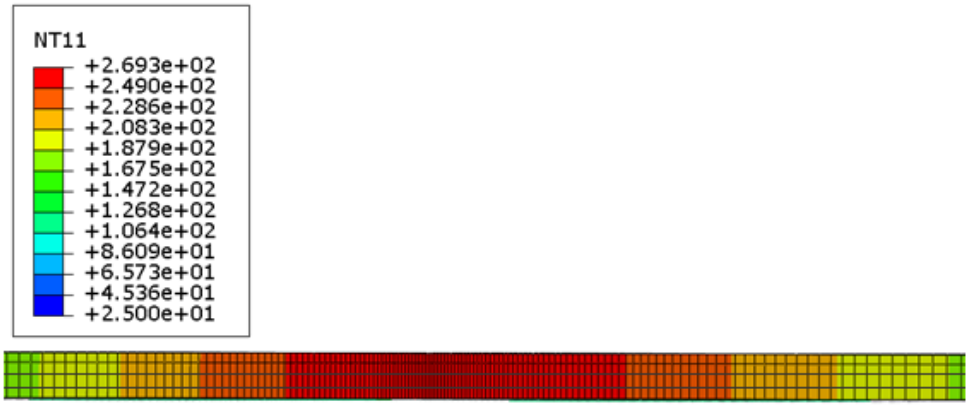

Fig. 4 Temperature contours at X-Y plane
(Laser power =210 W, Scanning speed=5.6 mm/s, focused on the St12 surface)

Figure 4 also shows the temperature contours at X-Y plane transverse to the laser scanning direction. According to the CIN heat source model maximum temperature is predicted at the

center of the laser beam. This figure shows that the center of the beam has a maximum temperature of around 269 °C. A slight increase in the joint width along with laser travelling direction can be predicted which indicates gradual increasing of heat absorption by metal during the joining process. Hence, the maximum bond width is anticipated at the endpoint of laser travelling direction. Investigation of temperature history over joining process demonstrates sharp heating rate at the start point and uniform heating rate at the end point of the laser traveling direction. Figure 5 depicts temperature history at the start point and end point of the laser traveling direction. The difference between heating rate of different points influences the pyrolysis of the Polycarbonate. While the start point reaches 250 ° C in less than a second it takes 2 seconds for the end point to reach the 250 ° C. The higher heating rates result in an increase in the decomposition temperature [23]. Although the start point and end point have the same linear energy their heating rate, bond width, and decomposion temperature are different. It is also understood that the temperature changes more rapidly at the metal interface because of the higher thermal conduction coefficient of the St12 than of the PC.

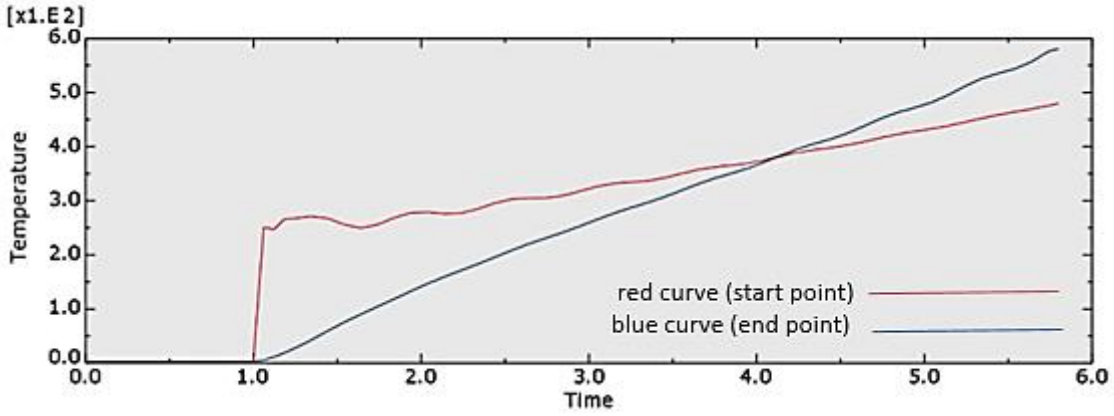

Fig. 5 Temperature history at start point (red curve) and end point (blue curve)

2-4- Experimental process and model verification

In heat-conduction joining (HCJ) of St12 and Polycarbonate, the metal part is heated to a relatively high temperature and melts the plastic interface. When the temperature reaches a higher temperature than the melting point of PC a joining pool is developed at the PC surface. While St12 and Polycarbonate laser joining, a chemical bonding is anticipated between iron oxide of the metal surface and molecules present in the polymer chains. Organic compounds tend to form aromatic compounds at high temperatures. In fact, when the temperature rises sufficiently, the polymer bonds are broken down by vibrational energy. Polymer chains are more liable to change their conformation and orientation towards the metal surface in the molten state to facilitate the formation of hydrogen bonds as a plausible form of interaction [8]. Hence, in the molten state, the polymer chains are likely to form hydrogen bonding as a secondary interaction [15]. Increasing the temperature of the polycarbonate in laser joining and generation of high pressure due to formation of the bubbles in the polymer provides suitable circumstances for hydrogen bonding between the hydrogen atoms of the polymer chains and the oxygen atoms from the iron oxide.

Several experiments are conducted to achieve a direct joint between Polycarbonate and St12 by a pulsed Nd: YAG ($\lambda = 1064$ nm) laser machine. Using pulsed Nd: YAG allows the flexibility of controlling the linear energy by adjusting the pulsed laser parameters [14]. The Heat-conduction joining configuration is employed in the experiments. The schematic of the St12 and Polycarbonate specimens is presented in Fig. 6. Specimens are get together in lap joint

configuration by a holding fixture. Laser frequency, pulse duration, laser scanning speed, and laser focal point are evaluated in order to study the feasibility of direct joint between Polycarbonate and St12. Different settings to obtain the dissimilar direct joint are reported in Table. 1.

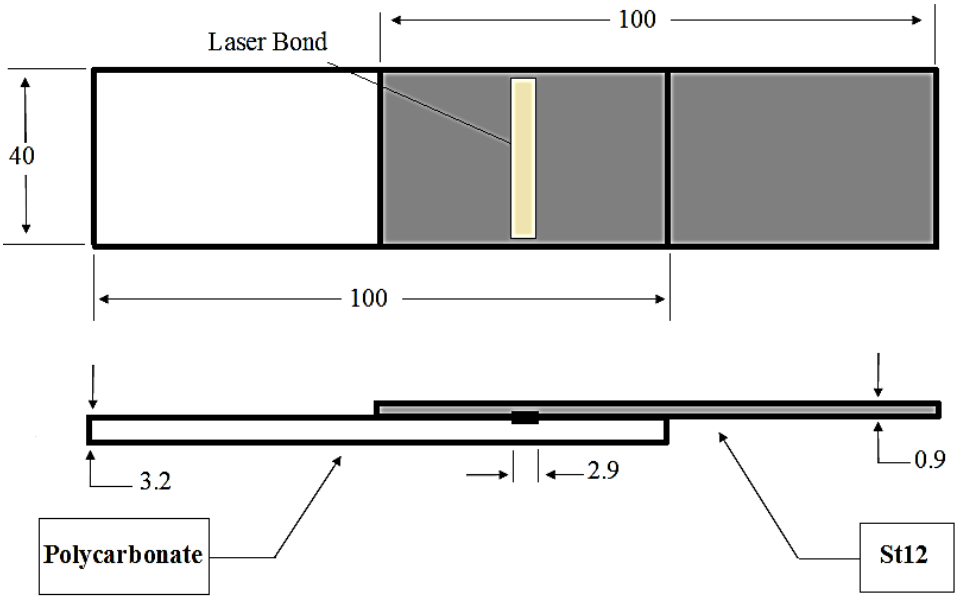

Fig. 6 Schematic of a St12/Polycarbonate samples

Table. 1 Settings in the feasibility study of St12 to Polycarbonate laser joining

Run	Pulse Duration(ms)	Frequency (Hz)	Focal Point (mm)	Power (W)	Speed (mm/s)	Linear Energy (J/mm)	Result
1	18	10	6	203	2	101.5	No bonding
2	16	10	6	189	2	94.5	No bonding
3	14	14	5	229	2.8	81.78	No bonding
4	10	19	5	223	2.8	79.64	No bonding
5	12	14	4.1	200	2.8	71.42	No bonding
6	10	19	4.1	206	3.4	66.47	No bonding
7	14	15	6	122	3	40.66	Partial bonding
8	14	15	6	122	2	61	No bonding
9	14	15	5	122	2	61	No bonding
10	6	20	4.1	210	2	105	No bonding
11	6	20	4.1	210	4	52.5	No bonding
12	6	20	4.1	210	5.6	37.5	Direct joint

In the most cases, the polymer on the metal-plastic interface was degraded, however, the materials are joined in the small area in the vicinity of the laser radiation line. Finally, Polycarbonate is joined to St12 by means of the Nd: YAG. The laser beam with a total power of 210 W and 6 ms pulse duration and 20 Hz frequency was focused on the St12 surface and the spot size was about 200 μm. A scanning speed of 5.6 mm/s is set to produce the 35.8 mm joint line and a bond width of 2.9 mm was measured. The St12 to Polycarbonate laser joining trials are displayed in Fig. 7. A power-meter is used to determine laser power at different settings. It can be noticed that the dissimilar joints can be obtainted at almost 40 J/mm linear energy. Moreover, numerous bubbles are observed in the joining area due to pyrolysis of the polymer. Figure 8 depicts the formation of several sub-milimeter bubbles in the Polycarbonate at the start point and end point of the joint. Pyrolysis of polymer can be defined as the

degradation reaction of solid phase into condensable and non-condensable volatiles and negligible char. The main gases released during the pyrolysis of polycarbonate are CO2, CH4, CO, H2O [23]. Although formation of the bubbles in the polymer is essential to form a dissimilar joint [16], large bubbles at the joint interface is not favourable because the bubbles at the interface reduce joining areas required to develop mechanical and chemical bonding.

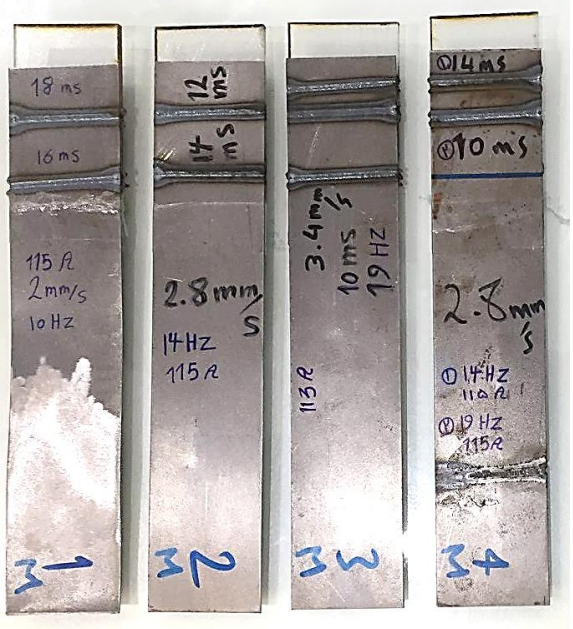

Fig. 7 St12 to Polycarbonate laser joining trials (width of samples = 40 mm)

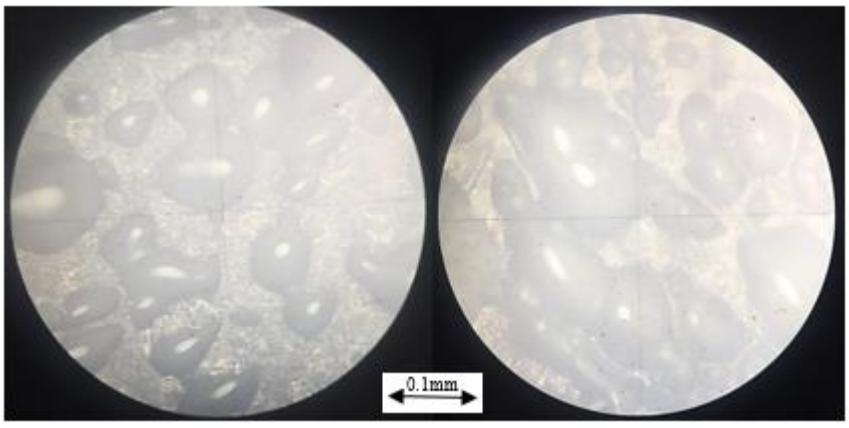

(a) **(b)**

Fig. 8 Bubbles in the Polycarbonate at a) start point and b) end point of the joint (100x magnification)

Figure 9 shows the length and width of the laser joint interface. As predicted there is a slight increase in the joint width along with the joint line. Table. 2 compares experimental bond width with simulated bond width at start, middle, and end points along with laser travelling direction shown in Fig. 9. The simulated results are analogous to the experimental results, hence the FE model is valid. As a consequence, the FE model can be used by Response Surface Method (RSM) to evaluate effects of different process parameters on bond width.

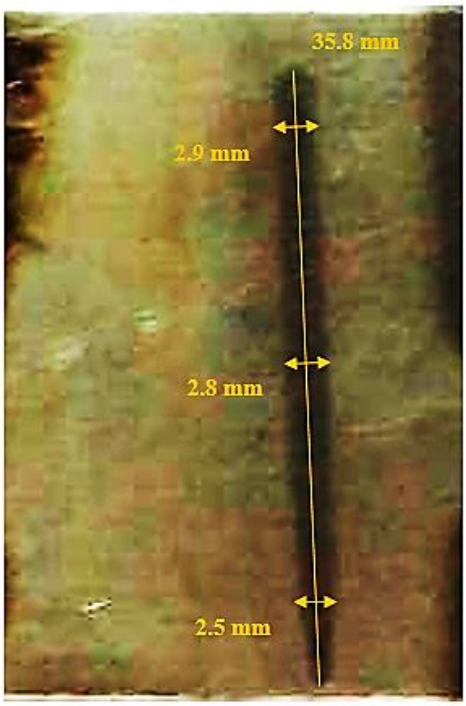

Fig. 9 Length and width of the laser joint interface (2x magnification)

Table. 2 Comparison of experimental and simulated bond width

point	Speed (mm/s)	Power (W)	Spot Size (µm)	Focal Point (mm)	Simulated bond width (mm)	Experimental bond width (mm)	Error (%)
Start	5.6	210	200	4.1	2.63	2.5	-5.2
Middle	5.6	210	200	4.1	3.05	2.8	-8.9
End	5.6	210	200	4.1	3.18	2.9	-9.6

RSM is an arranged and organized method to determine linkage between agents affecting a process and results. RSM design aims to quantify functional relations connecting one or more output responses and input factors [24]. The object is to discover links between results and inputs (parameters and responses) with a least error in the form of a mathematical model [25]. A functiona relating a response *Y* with the k levels of input variables is defined by [26]:

$$Y = f(x1, x2, \ldots, xk) + \mathcal{E} \tag{6}$$

Where $\mathcal{E}$ denotes the random error due to uncontrollable variables. To predict the response η, it is required to obtain a proper functional relationship between the independent variables and the response surface [27]. The second order polynomial equation can be used to predict the response *y* which is defined by the equation (7):

$$y = \beta_0 + \sum_{i=1}^{k} \beta_i x_i + \sum_{i=1}^{k} \beta_{ii} x_i^2 + \sum_{i} \sum_{j} \beta_{ij} x_i x_j + \varepsilon \tag{7}$$

In the dissimilar laser joining process, the laser power and laser scanning speed are the main factors influencing bond strength. Careful selection of laser joining parameters would reduce joining problems [28]. Response variables are average bond width (AW), delta bond width (DW), and maximum temperature (MT). Average bond width is the average of maximum bond width at the endpoint and minimum bond width at the start point of laser travelling direction. Delta bond width is the difference between maximum and minimum bond width. Maximum temperature is the maximum of temperature profile at the end point of laser travelling direction. The analysis is designed based on Central Composite Design (CCD) full replication with two factors five levels. Table. 3 shows levels of independent variables. The out puts and designed experiments of numerical simulation are displayed in Table. 4.

Table. 3 Levels of independent variables

Variable	Symbol	Unit	Levels				
			-2	-1	0	1	2
Laser Power	**P**	**W**	190	200	210	220	230
Laser Scanning Speed	**S**	**mm/s**	3.6	4.6	5.6	6.6	7.6

Table. 4 Design matrix and numerical results

Run	Input Variables		Output Responses		
	Laser Power	Laser Scanning Speed	Average Bond Width (AW)	Delta Bond Width (DW)	Maximum Temperature (MT)
1	0	-2	3.96	1.19	306
2	0	0	2.7	0.4	275
3	1	1	2.9	0.48	279
4	0	0	2.7	0.4	275
5	0	0	2.7	0.4	275
6	-1	1	0.97	0.18	239
7	0	0	2.7	0.4	275
8	-2	0	1.31	0.32	247
9	2	0	3.98	0.52	298
10	-1	-1	2.46	0.63	276
11	1	-1	3.93	0.72	299
12	0	2	2.25	0.13	263
13	0	0	2.7	0.4	275

3- Results and Discussion

FE thermal analysis results are employed to evaluate thermal phenomena in the joining process. Output responses are attained by FE predictions of maximum and minimum bond width at the end point and start point of laser travelling direction as well as maximum of temperature profile at the end point of laser scanning direction. The maximum temperature of Polycarbonate should be more than the crystalline melting temperature, but lower than the degradation temperature of the polymer [29]. The statistical analysis is conducted by Design-Expert V8 software. The ANOVA table or analysis of variance determines effects of independent variables on output responses. The ANOVA is made totally on the principle that the factors are fixed, not random and the design is crossed, not nested. It reports statistics such as Residual, Lack of Fit, and R-squared for evaluating the models. The Residual row shows how much variation in the response is still unexplained. Lack of Fit is the amount by which the model predictions deviate from observations. Pure Error is the difference between replicate runs. The R-Squared results confirm that predictive models are significant and whether these models can be used to explore the design space. The model F-Values quantify the contribution of the model terms on a response.

The p-value is a probability that measures the evidence against the null hypothesis. Lower probabilities provide stronger evidence against the null hypothesis. If the p-value is very small (less than 0.05 by default), then the source is significant.

3-1- Average bond width

The ANOVA table reveals that power and scanning speed of laser are the most significant controlled variables for average bond width. Table. 5 demonstrates ANOVA analysis for average bond width.

Table. 5 Average bond width Analysis of variance (ANOVA)

Source	*Sum of Squares*	*Df*	*Mean Square*	*F Value*	*p-value Probe > F*
Model	80.30	3	26.77	145.78	< 0.0001
P	51.23	1	51.23	279.01	< 0.0001
S	26.31	1	26.31	143.31	< 0.0001
S^2	2.76	1	2.76	15.02	0.0038
Residual	1.65	9	0.18		
Lack of Fit	1.65	5	0.33		
Pure Error	0.000	4	0.000		
Cor Total	81.95	12			
	Adj R-Squared	0.9798	R-Squared	0.9731	

The equation (8) is predictive model of average bond width and in terms of coded factors:

$$(\text{Average Bond Width})^{1.61} = +4.94 + 2.07P - 1.48S + 0.33S^2 \quad (8)$$

The coded equation is helpful for identifying the relative significance of the terms by comparing the terms coefficients. Figure 10 depicts the average bond width perturbation plot. The perturbation plot helps to compare the effect of all the terms in the central point in the design space. The average bond width is plotted by modifying only one term over its range while holding the other factor constant. Line A shows sensitivity of average bond width to laser power and line B shows sensitivity of average bond width to laser scanning speed. Figure 11 demonstrates effects of laser power and laser scanning speed on average bond width. Results show that increasing laser power leads to a wider bond width and increasing laser scanning speed results in narrower bond width [22]. It can be inferred, increasing linear energy leads to higher heat absorption by metal surface which results in a wider bond; higher linear energy leads to decomposition of the polymer [11]. Figure 12 shows normal probability plot of the studentized residuals which is a tool to chech whether the residuals follow a normal distribution, in which case the dots in the plot should follow a straight line.

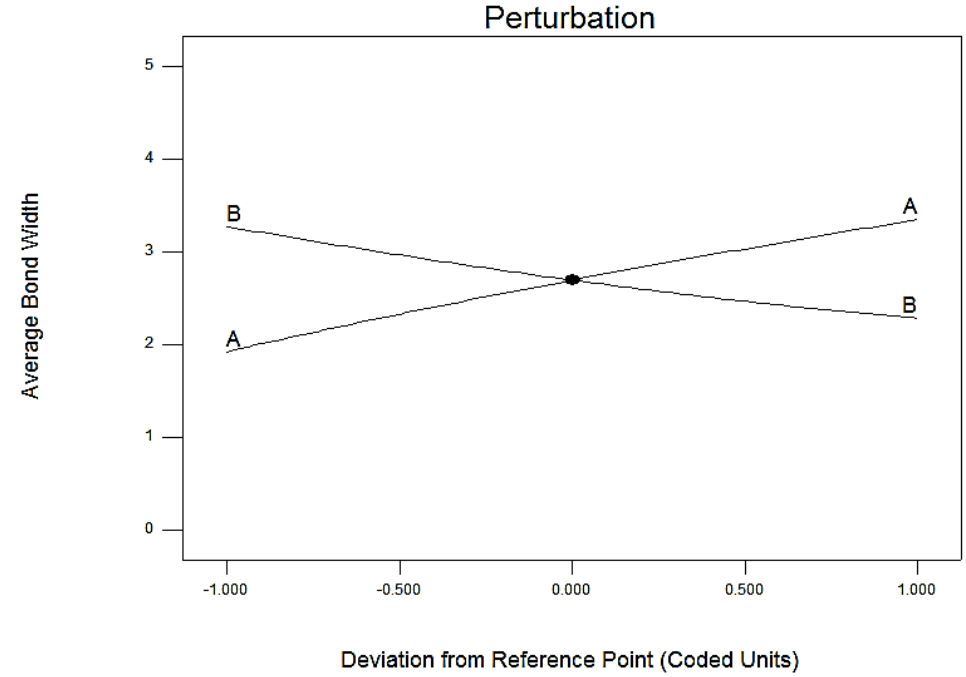

Fig. 10 Perturbation plot of average bond width

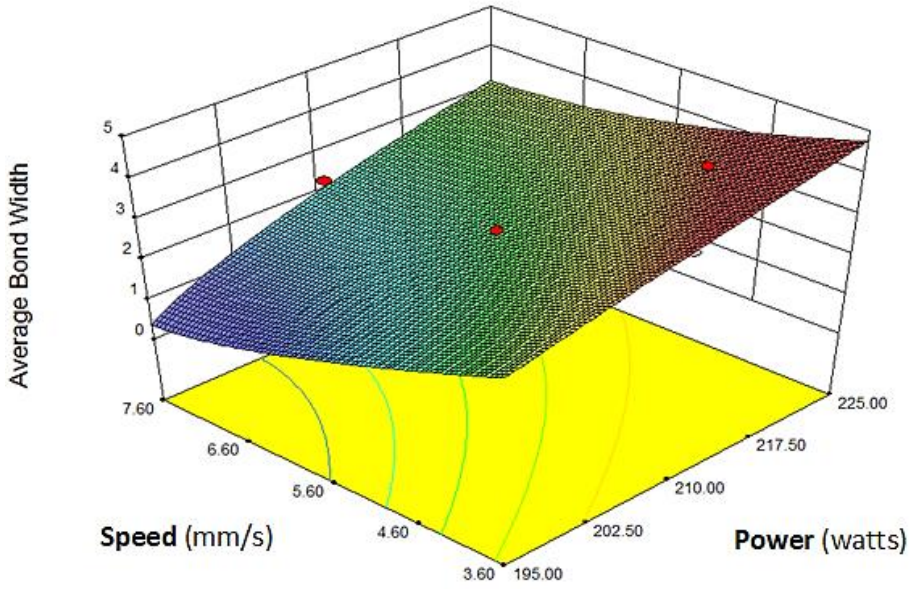

Fig. 11 3D surface plot of average bond width

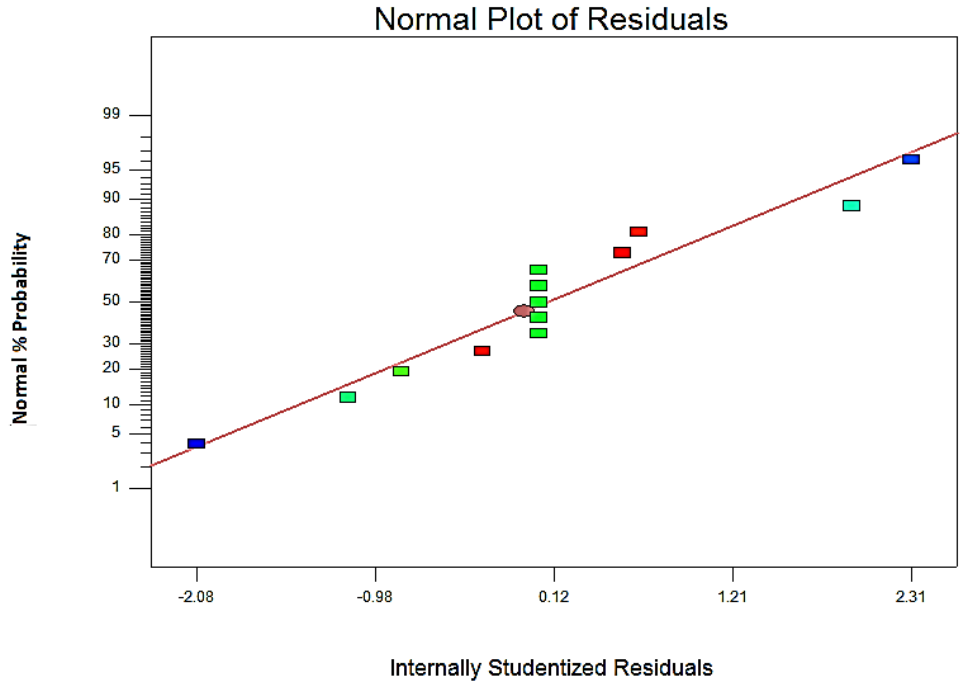

Fig. 12 Normal plot of residuals

3-2- Delta bond width

The ANOVA table discloses laser scanning speed and laser power are the most influential parameters on delta bond width. Table. 6 demonstrate ANOVA analysis for delta bond width.

Table. 6 Delta bond width analysis of variance (ANOVA)

Source	Sum of Squares	Df	Mean Square	F Value	p-value Probe > F
Model	0.016	3	5.185E-003	73.50	< 0.0001
P	1.540E-003	1	1.540E-003	21.84	0.0012
S	0.013	1	0.013	188.46	< 0.0001
PS	7.274E-004	1	7.274E-004	10.31	0.0106
Residual	6.349E-004	9	7.054E-005		
Lack of Fit	6.349E-004	5	1.270E-004		
Pure Error	0.000	4	0.000		
Cor Total	0.016	12			
	Adj R-Squared	0.9608	R-Squared	0.9477	

The equation (9) shows predictive model of delta bond width in phrases of coded factors:

$$(\text{Delta Bond Width})^{0.07} = +0.94 + 0.011P - 0.033S + 0.013PS \quad (9)$$

Figure 13 depicts perturbation plot of delta bond width. Perturbation plot indicates that delta bond width is more sensitive to scanning speed of laser. Figure 14 shows effects of laser power on delta bond width. In fact, increasing scanning speed at lower power results in lower linear energy which leads to smaller delta bond width [24]. Figure 15 shows probability plot of the residuals. Some moderate scatter even with normal data is expected.

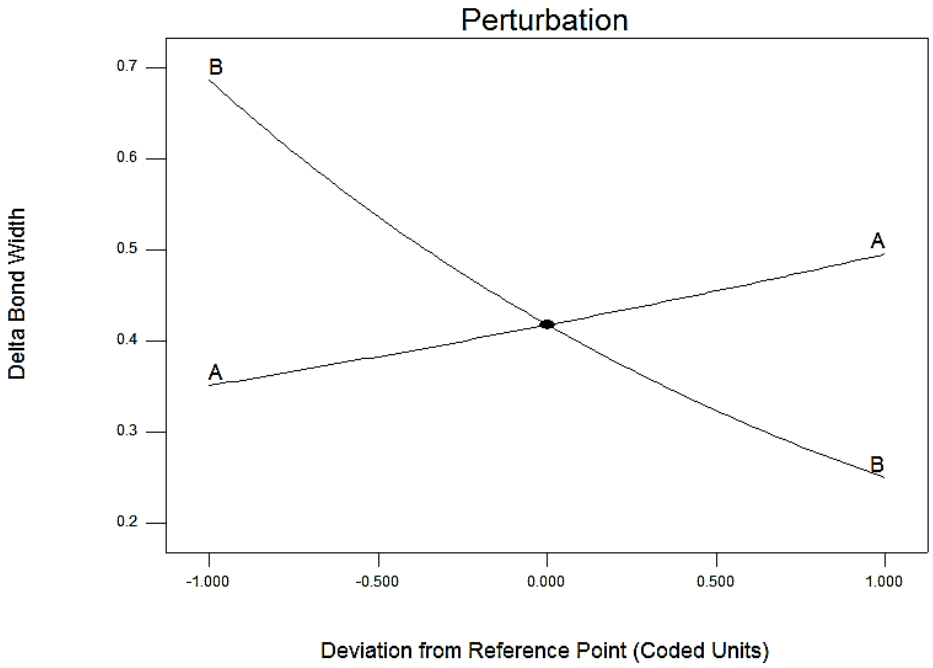

Fig. 13 Perturbation plot of delta bond width

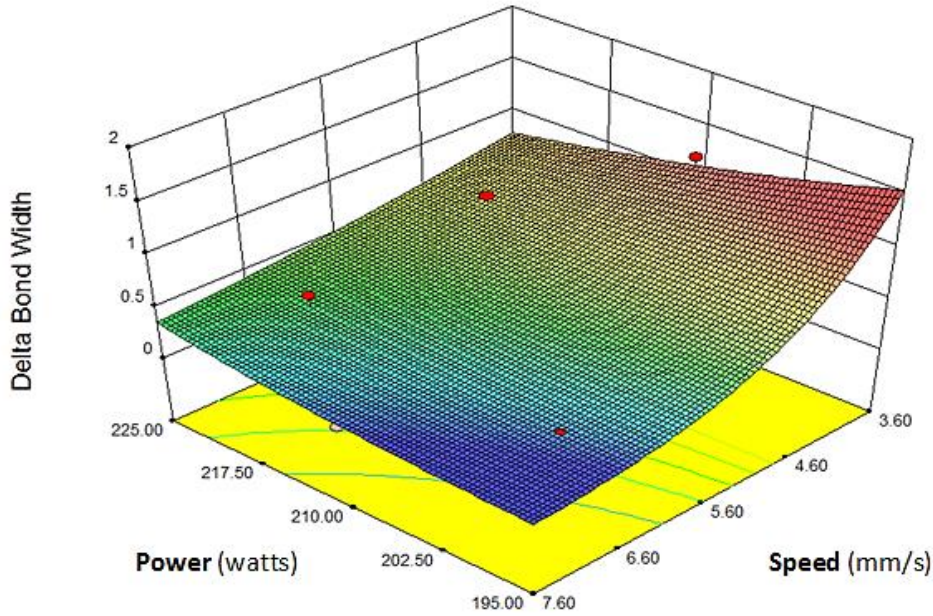

Fig. 14 Delta bond width 3D surface plot

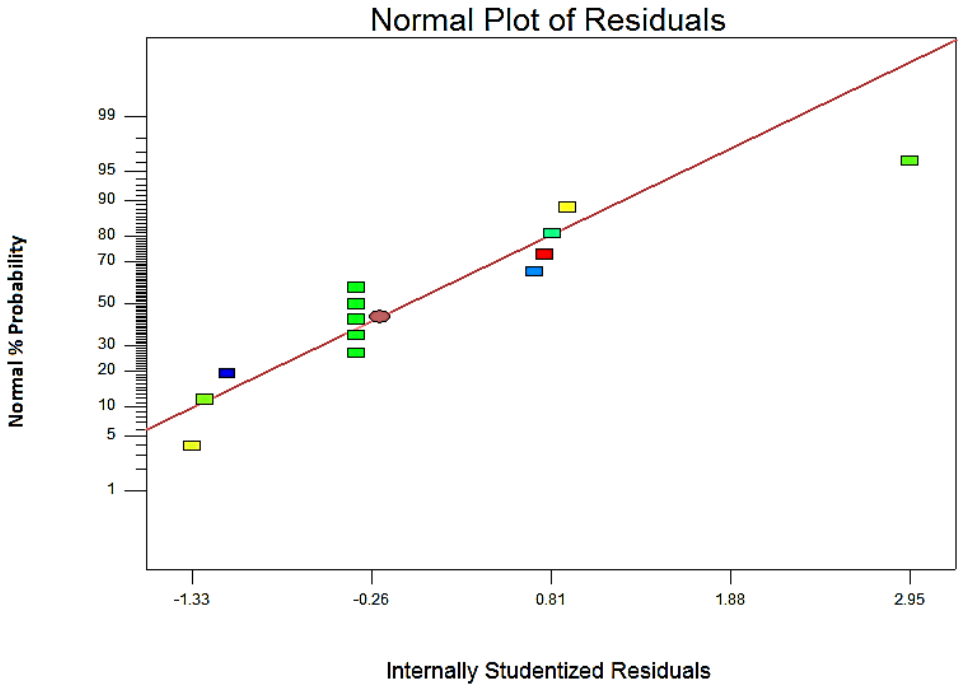

Fig. 15 Normal plot of residuals

3-3- Maximum of temperature profile

The ANOVA table depicts power and scanning speed of laser are the most effective parameters on maximum of temperature profile. Table. 7 demonstrate ANOVA analysis for maximum of temperature profile.

Table. 7 Maximum of temperature profile Analysis of variance (ANOVA)

Source	Sum of Squares	Df	Mean Square	F Value	p-value Probe > F
Model	2.158E+014	4	5.394E+013	154.94	< 0.0001
P	1.114E+014	1	1.114E+014	319.94	< 0.0001
S	9.245E+013	1	9.245E+013	265.54	< 0.0001
PS	1.392E+012	1	1.392E+012	4.00	0.0806
S^2	1.054E+013	1	1.054E+013	30.27	0.0006
Residual	2.785E+012	8	3.482E+011		
Lack of Fit	2.785E+012	4	6.963E+011		
Pure Error	0.000	4	0.000		
Cor Total	2.186E+014	12			
	Adj R-Squared	0.9608	R-Squared	0.9477	

The equation (10) is predictive model of delta bond width in terms of coded factors:

$$(\text{Maximum Temperature})^3 = +2.059E+007 + 3.047E+006P - 2.776E+006\ S + 5.898E+005\ PS + 6.503E+005\ S^2 \quad (10)$$

The main advantage of investigating the maximum temperature is to anticipate the process parameters that instigate an appropriate range of polymer temperature. If maximum temperature is lower than the melting point of PC there will be no bond between St12 and PC. If topmost temperature is higher than decomposition point of PC there will be decomposition points on the polymer [29]. Figure 16 displays the maximum of temperature profile perturbation plot. The perturbation plot denotes that maximum of temperature profile is more sensitive to input

variables than average bond width. Figure 17 represents effects of power on maximum of temperature profile. Results illustrate that decreasing scanning speed and raising power result in increasing the maximum of temperature profile as proofed by the reference [22]. Figure 18 shows the studentized residuals normal probability plot.

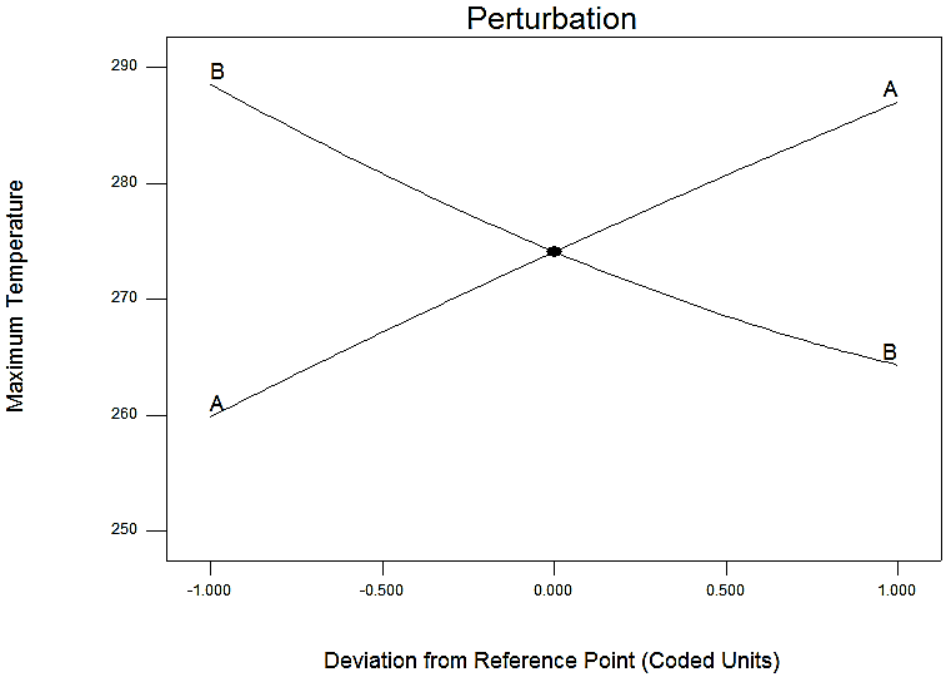

Fig. 16 Maximum of temperature profile Perturbation plot

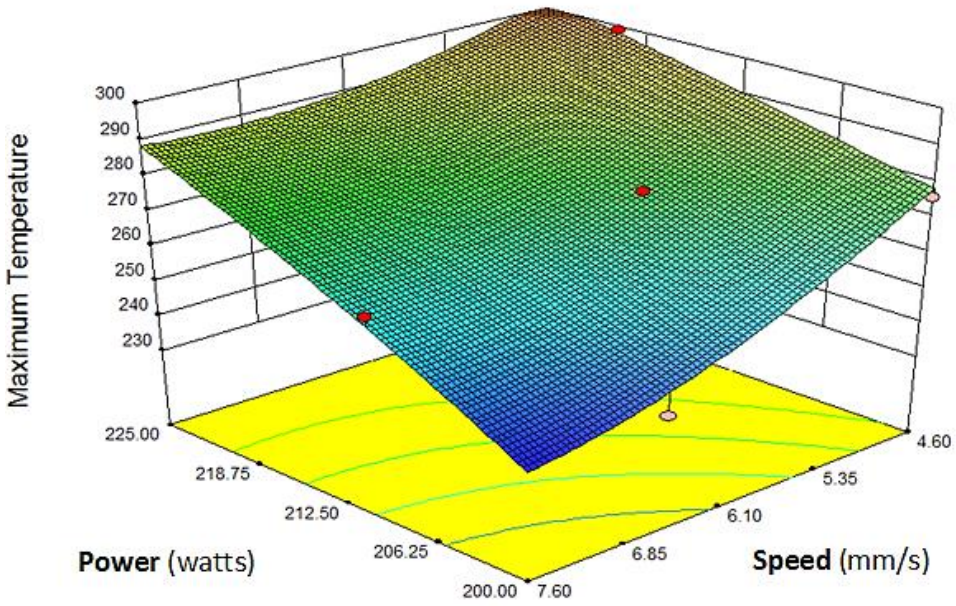

Fig. 17 Maximum of temperature profile 3D surface plot

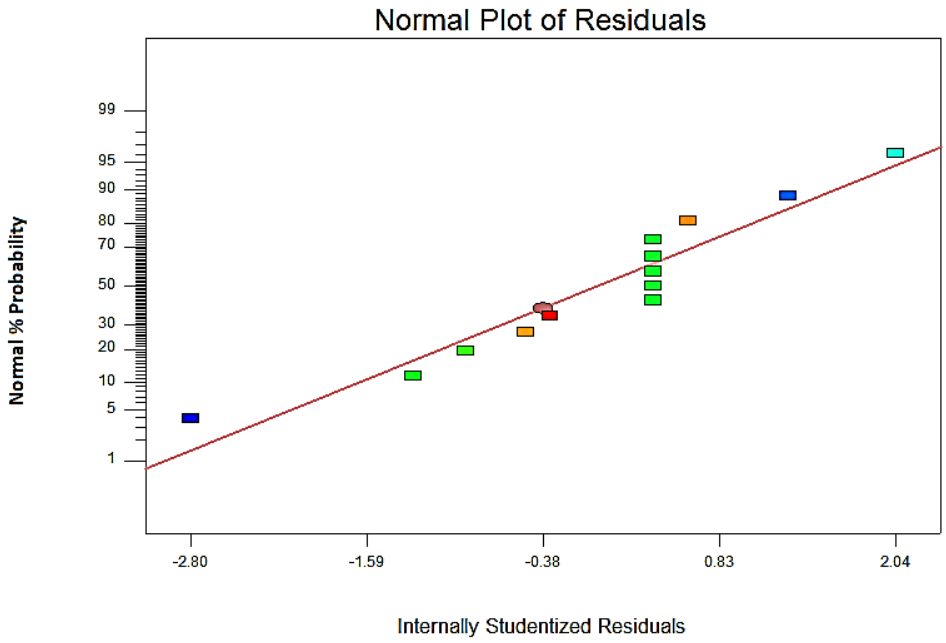

Fig. 18 Normal plot of residuals

3-4- Optimization

Wider bond width can result in higher strength in the dissimilar joint and also non-uniform bond width along with the joint can lead to unbalanced resistance against loading condition. Therefore, optimization objective is to attain maximum average bond width with minimum delta bond width. Table. 8 shows optimization criteria. The maximum of temperature profile should be between melting point and decomposition point of the Polycarbonate to ensure of achieving the dissimilar joint without decomposition of Polycarbonate. Therefore, the melting point of Polycarbonate is considered as lower limit of maximum temperature and decomposition point is considered as upper limit in the optimization criteria.

The optimized setting to achieve optimization objective are reported in Table. 8. The optimized solution is simulated by Abaqus to compare results of the FE analysis with RSM predictions. Table. 9 also compares the results of the FE software with RSM predictions. Results show there is a suitable agreement between out puts of the two methods. Figure 19 shows overlay plot which contains the contour plots from each response laid on top of each other. On each contour plot, the desirable area is yellow and undesirable area is grayed-out. The remained yellow area defines the final optimal ranges of factors. Therefore, higher power and medium scanning speed of laser should be applied to achieve maximum average bond width with minimum delta bond width. Nevertheless, more consideration should be given to avoid decomposition of PC at the laser joint center and at the end of laser travelling direction because there is no bond at the decomposition points between PC and St12.

Table. 8 Optimization criteria

Parameters/Responses		Name	Goal	Lower limit	Upper limit	Lower Weight	Upper Weight	Importance
Parameters		Laser power	is in rang	190	230	1	1	-
		Laser scanning speed	is in rang	3.6	7.6	1	1	-
Responses	Criteria	Average bond width	Maximum	0.97	4.1	1	1	3
		Delta bond width	Minimum	0.5	1.19	1	1	3
		Maximum temperature	is in rang	215	377	1	1	3

Table. 9 Comparison between results of the FE software with RSM

Solution	Optimized setting		Desirability	Type of results	Responses		
	Power	Speed			AW	DW	MT
				Abaqus results	3.91	0.68	283
	230	5.21	0.918	RSM results	4.1	0.6085	301.47
				Error	-4.8 %	10.5%	-6.5%

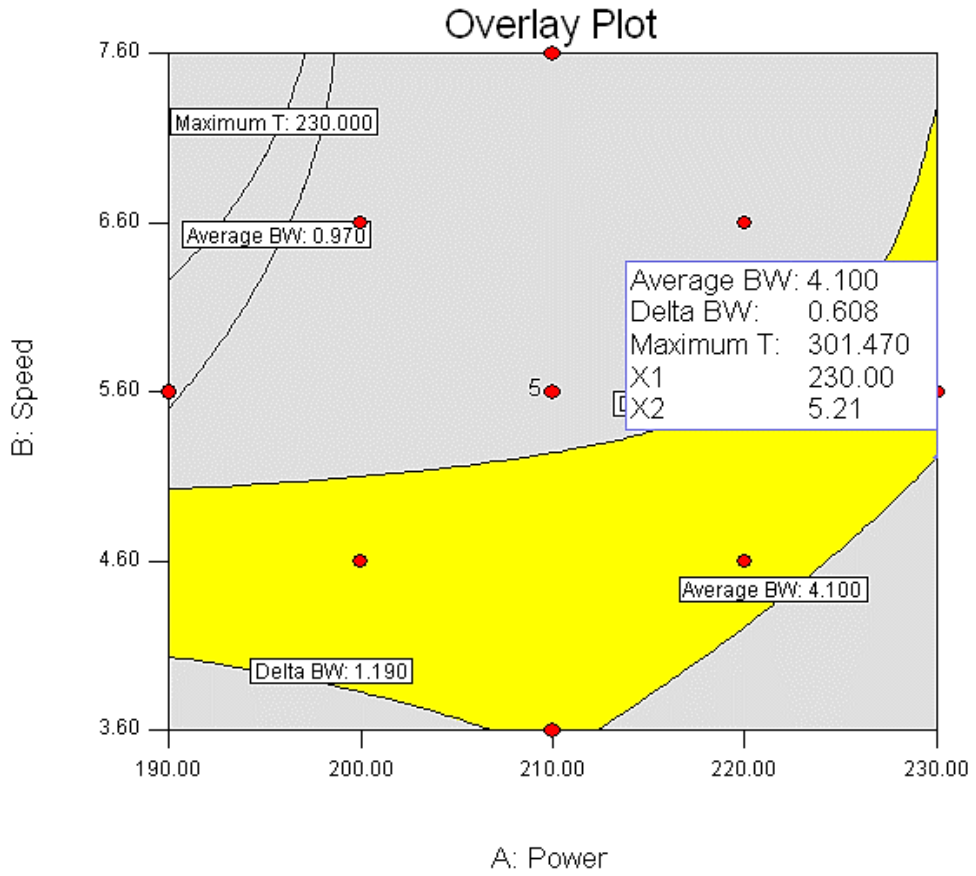

Fig. 19 Overlay contour plot

4- Conclusions

In this research, laser joining of St12 and Polycabonate is achieved by empirical experiments. A FE model is developed by Abaqus software to check effects of power and scanning speed of laser on the average bond width, delta bond width, and maximum of temperature profile. From the obtained results, the following conclusions are mentioned:

1. Results confirm formation of bonding between St12 and Polycabonate by laser joining. The joint width increases along with the laser travelling direction. Formation of large size bubbles at the interface of the joint, however, leads to more non-joined areas.
2. Comparison between experimental bond width with simulated bond width at start, middle, and end points along with laser travelling direction indicates that finite elememt method is fairly capable of predicting joint width.
3. The heating rate at the start point is much more than the end point of the laser traveling direction. Therefore, decomposition temperature at the start point is higher than the end point of laser traveling direction.

4. The statistical analysis denoted that power and scanning speed of laser are the most significant parameters on both average bond width and maximum of temperature profile. Laser scanning speed and power of laser are the most influential parameters on delta bond width.
5. The obtained process parameters to gain desired and optimum results are laser power = 230 W and laser scanning speed = 5.21mm/s with 44.15 J/mm linear energy. It seems that couples of joint lines are needed to obtain a practical joint between St12 and Polycarbonate by a Nd:YAG laser because the process window required to achieve a sound dissimilar joint (without any decomposition of the polymer) does not allow implementation of higher linear energy to attain a wider bond width.

9- References

[1] A. Roesner, S. Scheik, A. Olowinsky, A. Gillnera, U. Reisgen, M. Schleser, Laser Assisted Joining of Plastic Metal Hybrids, Physics Procedia. 12 (2011) 370–377.

[2] M. Moradi, O. Mehrabi, T. Azdast, K.Y. Benyounis, Enhancement of low power CO2 laser cutting process for injection molded polycarbonate, Optics & Laser Technology. 96 (2017) 208-218.

[3] M. Moradi, D. Ghorbani, M. Karami Moghadam, M. Kazazi, F. Rouzbahani, Sh. Karazie, Nd:YAG laser hardening of AISI 410 stainless steel: microstructural evaluation, mechanical properties, and corrosion behavior, Journal of Alloys and Compounds, 795: 30, (2019) 213-222.

[4] Amir Hosein Faraji, Mahmoud Moradi, Massoud Goodarzi, Pietro Colucci, Carmine Maletta (2017) An investigation on capability of hybrid Nd:YAG laser-TIG welding technology for AA2198 Al-Li alloy. Optics and Lasers in Engineering. 96 (2017) 1-6.

[5] Mahmoud Moradi, Majid Ghoreishi and Ali Khorram, Process and Outcome Comparison Between Laser, Tungsten Inert Gas (TIG) and Laser-TIG Hybrid Welding. Journal of lasers in Engineering, 39(3-6) (2018) 379-391.

[6] A. khorram, A. Jafari, M. Moradi, Laser brazing of 321 and 410 stainless steels using BNi-2 nickel-based filler metal, Modares Mechanical Engineering. 17 (1) (2017) 129-135.

[7] S. Katayama, Handbook of laser welding technologies. Woodhead Publishing Limited. (2013)

[8] S. Katayama. Y. Kawahito, Laser direct joining of metal and plastic, Scripta Materialia. 59 (2008) 1247–1250.

[9] M. Wahbaa. Y. Kawahitoc. S. Katayama, Laser direct joining of AZ91D thixomolded Mg alloy and amorphous polyethylene terephthalate, Journal of Materials Processing Technology. 211 (2011) 1166-1174.

[10] Y. Kawahito. K. Nishimoto. S. Katayama, LAMP Joining between Ceramic and Plastic, Physics Procedia. 12 (2011) 174–178.

[11] A. Bauernhuber. T. Markovits, Investigating thermal interactions in the case of laser assisted joining of PMMA plastic and steel, Physics Procedia. 56 (2014) 811–817.

[12] J.P. Bergmann. M. Stambke, Potential of laser-manufactured polymer-metal hybrid joints, Physics Procedia. 39 (2012) 84–91.

[13] J. Kwang-Woon. K. Yousuke. K. Seiji, Laser Direct Joining of CFRP to Metal or Engineering Plastic, Transactions of JWRI. 42 (2013) 5-8.

[14] Furat I.Hussein, E.Akman, B.Genc Oztoprak, M.Gunes, O. Gundogdu, E. Kacar, K.I.Hajim, A. Demir, Evaluation of PMMA joining to stainless steel 304 using pulsed NdYAG laser, Optics &Laser Technology. 49 (2013) 143–152.

[15] C. Lamberti. T. Solchenbach. P.Plapper. W. Possart, Laser Assisted Joining of Hybrid Polyamide-Aluminum Structures, Physics Procedia. 56 (2014) 845–853.

[16] M. Kubiak, W. Piekarska, R. Parkitny, Theoretical study on thermal and structural phenomena in thin elements heated by a laser beam, Archives of Mechanics. 67(1) (2015) 3–24.

[17] T. Mościcki, J. Hoffman, Z. Szymański, Modelling of plasma formation during nanosecond laser ablation, Archives of Mechanics. 63(2) (2011) 99–116.

[18] W. Piekarska, W. Kubiak, M. Saternus, Z. Saternus, Computer simulation of temperature field in laser beam welded lap joint. 32(1) (2012) 37-45.

[19] E. Ranatowski, Thermal modelling of laser welding. Part I: The physical basis of laser welding, Advances in Materials Science. 1 (2003) 34–40.
[20] F. I. Hussein, K. N. Salloomi, E. Akman, K. I. Hajim and A. Demir, Finite element thermal analysis for PMMA/st.st.304 laser direct joining, Optics & Laser Technology. 87 (2017) 64-71.
[21] Kh.Farhangdoust, H.Kamankesh, Three-dimensional finite element analysis of the front cross member of the Peugeot 405, World Academy of Science, Engineering and Technology. 68 (2010) 360-364.
[22] F. Lambiase, S. Gennab, Laser-assisted direct joining of AISI304 stainless steel with polycarbonate sheets: Thermal analysis, mechanical characterization, and bonds, Optics & Laser Technology. 88 (2017) 205–214.
[23] E. Apaydin-Varol, S. Polat, A. E. Putun, Pyrolysis kinetics and thermal decomposition behavior of polycarbonate - a TGA-FTIR study, Thermal Science 18(3) (2014) 833-842
[24] M.S. Shaikh Mohammad Meiabadi, A. Kazerooni, M. Moradi, Numerical Analysis of Laser-assisted Ti to Polyimide Welding Using a Statistical Approach, International Journal of Laser Science: Fundamental Theory and Analytical Methods. 1 (2018) 185–205
[25] M. Moradi, H. Arabi, M. Shamsborhan, Multi-objective optimization of high power diode laser surface hardening process of AISI 410 by means of RSM and desirability approach, Opt. – Int. J. Light Electron. 202 (February), 2020. 163619.
[26] M. Moradi and M. KaramiMoghadam, High power diode laser surface hardening of AISI 4130; statistical modelling and optimization. Optics & Laser Technology. 111 (April), 554-570.
[27] M. Moradi, H. Abdollahi, Statistical Modelling and Optimization of the Laser Percussion Microdrilling of Thin Sheet stainless Steel, Lasers in Engineering 40 (4-6), (2018)375-393.
[28] Y. Farazila, M. Fadzil, M. Hamdi A brief review: Laser joining of polymer-metal structures, ASEAN Engineering Journal Part A. 2(2) (2012) 5-11.
[29] F. Lambiase, S. Genna, R. Kant, A procedure for calibration and validation of FE modelling of laser-assisted metal to polymer direct joining, Optics and Laser Technology 98 (2018) 363–372

Nomenclature

Q_L	Laser beam power
η_L	Laser efficiency
K_Z	Heat source power exponent
k	Beam focus coefficient
s	Heat source beam penetration depth
r_0	Beam radius
T	Temperature (K)
t	Time (seconds)
ρ	Material density(kg/m^3)
c	Specific heat capacity(J/(kgK))
kn	Thermal conductivities(W/(m K)
Q	Heat generation rate in per unit volume (W/(mK))
v	Velocity of laser (m/s)
q	Heat flux (W/m^2)
h_{conv}	Convection heat transfer coefficient (W/m^2 K)
σ	Stefan–Boltzmann constant(5.67×10^{-8} W/m^2 K^4)
T_0	Ambient temperature (K)
P	Laser power (W)
S	Laser scanning speed (mm/min)
$\mathcal{E}$	Random experimental error